Heritage Science

RESEARCH

Open Access

Selective damage induced by pigment-medium interactions in a Neoplasticist oil canvas painting: *Composition dans le cône avec couleur orange* by G. Vantongerloo (1929)

Francesca Caterina Izzo[1†], Margherita Gnemmi[1†], Miguel Ángel Herrero-Cortell[2], Ana María García-Castillo[2], María Teresa Martínez-López[3] and Laura Fuster-López[2*]

Abstract

This research focuses on the study of pigment-medium interactions in the film forming, ageing and degradation mechanisms of modern white oil paints observed in the Neoplasticist painting *Composition dans le cône avec couleur orange* by G. Vantongerloo (1929), conserved in the *Institut Valencià d'Art Modern* (IVAM). The observation of selective vertical cracks and the significant presence of protrusions in the painting suggested that the observed degradation phenomena were specific to the coloured area. To understand the composition of pigments governing the film formation processes and later degradation phenomena in the oil paint films, a hybrid experimental approach was taken, aimed at understanding the physical, chemical and mechanical mechanisms involved. For this purpose, digital portable microscopy and multiband imaging analyses were carried out. Furthermore, the technical study involved the use of micro-invasive analysis such as μ-Raman, ATR-FTIR spectroscopy and GC–MS analysis for a more comprehensive understanding of the nature of the binding media and products resulting from the auto-oxidation, film-forming, hydrolysis, and degradation processes of the lipidic binding media. The results obtained suggest that on-going degradation phenomena are closely linked to the chemical interaction between pigment and binding medium.

Keywords Vantongerloo, Neoplasticism, Pigment-medium interaction, Protrusions, Cracks, Failure mechanisms

Introduction

Neoplasticism is an Avant-garde art theory that originated in 1917 and was mainly developed by Dutch De Stijl artists. The most prominent proponents of this theory were Theo van Doesburg (1883–1931) and Piet Mondrian (1872–1944), who were able to use abstraction as a means of expression, albeit with different techniques and results [1]. They wanted to demonstrate the possibility of penetrating the essence of matter and finding new meanings and new keys to interpretation [2], an impulse dictated by the search for a utopian dimension to transform the social and political

†F. C. Izzo and M. Gnemmi equally contributed too this work.

*Correspondence:
Laura Fuster-López
laufuslo@crbc.upv.es
[1] Department of Environmental Sciences, Informatics and Statistics, Ca' Foscari University of Venice, Venice, Italy
[2] Universitat Politècnica de València, Instituto Universitario de Restauración del Patrimonio, Valencia, Spain
[3] IVAM, Institut Valencià d'Art Modern, Valencia, Spain

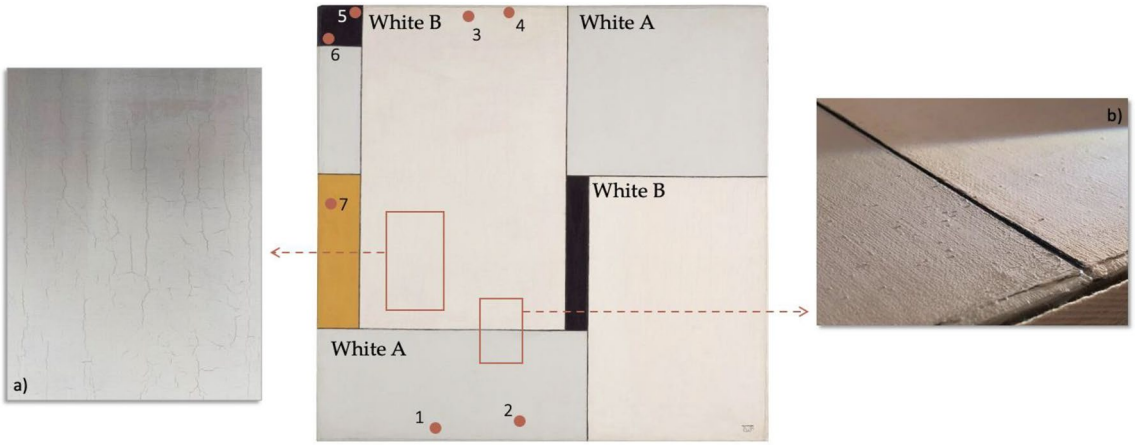

Fig. 1 *Composition dans le cône avec couleur orange* (1929) by Georges Vantongerloo. Oil on canvas (60.8 cm × 61.6 cm) conserved in Institut Valencià d'Art Modern (IVAM). The darker white is indicated as white A; the lighter white is indicated as white B. The dots represent the selected sampling areas; the rectangles highlight two points of interest: **a** crack patterns in the white B area; **b** protrusions only observed in-between white A and white B

Fig. 2 Diagrams presenting the typology and the damage are included in the conservation reports dated 2003 and 2015

reality characterised by the First World War. Abstract geometry, thus, became the means to realise a new way of seeing the world. Georges Vantongerloo (1886–1965) is one of the Neoplasticist artists who better reflected the scientific conception of art: he focused on the search for pure colour and contrast as perceptual and physical phenomena, to produce a rhythm in observation [3]. One of his masterpieces is *Composition dans le cône avec couleur orange* (1929), at IVAM (Fig. 1). In this canvas painting, the choice of shapes and colours resulted in a balanced and dynamic composition with homogeneous geometric areas made with plane colours including one yellow, one black and two different whites [4].

Thanks to the detailed condition reports produced by the IVAM over the years, it was possible to reconstruct the painting's conservation history (Fig. 2). The first conservation treatment took place in 1999. Localized forms of mechanical degradation (e.g., abrasion, cracks, colour variation) were reported over time (reports dated 2003, 2010, and 2018) and new cracks were observed and documented. In 2021, a thorough examination of the painting revealed the propagation of already existing cracks and the formation of new ones.

There were protrusions in the darker white area (white A) and visible and pronounced vertical cracks in the lighter white area (white B), as it can be seen in Fig. 1.

These signs of degradation were less evident in the yellow areas and absent in the black ones. Although the overall condition was rather good, different degradation phenomena occurred. Especially relevant is the fact that damage is distinctive as a function of the coloured areas: this suggests that the actual condition of the painting might be governed by the intrinsic nature of the painting materials and not necessarily environmentally-induced. It is from these observations and assumptions that the research that is the subject of this article was born, under the framework of MIMO[1] project which aims to connect the chemical nature of oil paint colours with their drying mechanisms which may lead to several degradation phenomena.

Starting from significant literature [5, 6], a hybrid experimental approach was chosen, aimed at understanding the physical, chemical and mechanical mechanisms involved. Thus, the artist's material choices were correlated to the damage observed and allowed to gain an insight into the role pigment-medium interactions played in the drying, film-forming, aging, and degradation processes of modern oil paints.

Materials and methods

Digital portable microscopy

A Dinolite® polarised microscope, model AM4815ZT equipped with a 1.3 megapixel sensor (1280×1024 pixels and 20 ~ 220 magnification) was used to obtain surface microscopy images. The built-in adjustable polarizer reduces flare on bright samples, especially when working with dark samples. All photographs were processed with Dinolite® software and the scale was always indicated graphically.

The images obtained made it possible to record the different cracks in the various coloured areas of the painting and to analyse their different patterns. In particular, these images allowed a detailed study of the different morphological aspects of the cracks in order to make an objective comparison between them.

Multi-band technical imaging

A 'full spectrum' digital Nikon® D800 camera (36 MP, CMOS sensor, sensitivity between 300 and 1100 nm) with a Nikon Nikkor 50 mm 1:1 coupled lens was used. A CHSOS Robertina® 52 mm filter set was adopted for shooting the different images.

To obtain VIS, and IR images, two halogen lamps (800W) with a diffuser were used, while for transillumination and trans-irradiation techniques only one lamp was used, located on the back of the canvas, at a distance of 80 cm, coupling a diffuser.

For UVL, IRL, and UVR a CHSOS Fabrizio UV high-Flux 365 nm LED lamp was used (filtered and exclusively with UV passage and cut-off of the VIS-IR emission).

To calibrate the images, a CHSOS card, consisting of an AIC PhD card [7], which incorporates pigmentary additions that respond in IR and UV bands, was used.

Images were taken in RAW and colour-corrected by white balance, using the N8 neutral grey of the AIC card. Also, fixed exposure: N8 150 ± 5 for VIS. The same gray was adopted in the correction of other images 100 ± 5 for IR, and 50 for UVR [8, 9].

To compare the behaviour of the colours along the spectrum, a pigment checker table ad hoc was created and contains 63 common historical pigments bound in oil paint [10].

Sampling

Seven samples (with an average weight of 0.5 mg) were collected and allowed spectroscopic and chromatographic analyses in order to identify the materials chosen by the artist and to understand the physical and chemical degradation phenomena taking place. The sampling areas are indicated in Fig. 1.

During the sampling campaign, in situ observations were made using a Wood lamp and a digital portable microscope, both in visible and UV light. These allowed to highlight the preparatory layer underneath the painted layers. In particular, a bright yellow UVfluorescence was observed on the back of all samples,where the preparatory layer could be identified. It was therefore possible to assume that the back of the samples corresponded to the preparatory layer (Fig. 3).

Attenuated total reflectance Fourier-transform infrared spectrophotometry (ATR-FTIR)

The ATR-FTIR analyses were carried out on all collected samples, both in the recto and verso of the fragments, in order to identify the composition of the pictorial materials from the paint layers (binding media, pigments and the presence of any additives), groundings (where present on the back of the samples) and degradation products.

Attenuated total reflectance Fourier-transform Infrared spectrophotometry analyses were acquired with a Bruker Optics Alpha spectrophotometer in ATR mode, with a diamond crystal capable of investigating a sample area of 0.75 mm at a depth of around 1 µm [11, 12]. The spectrometer was equipped with a Pt/SiC global source, a RockSolid interferometer (with gold mirrors), and a deuterated triglycine sulphate (DLaTGS) detector, operating at room temperature and giving a linear response in the spectral range between 7500 and 375 cm^{-1}. Spectra were

[1] "Metal Ion Migration mechanisms in Oil paints drying and degradation" (PID 2019-106616 GB-100 project granted by MCIN/ AEI /10.13039/501100011033).

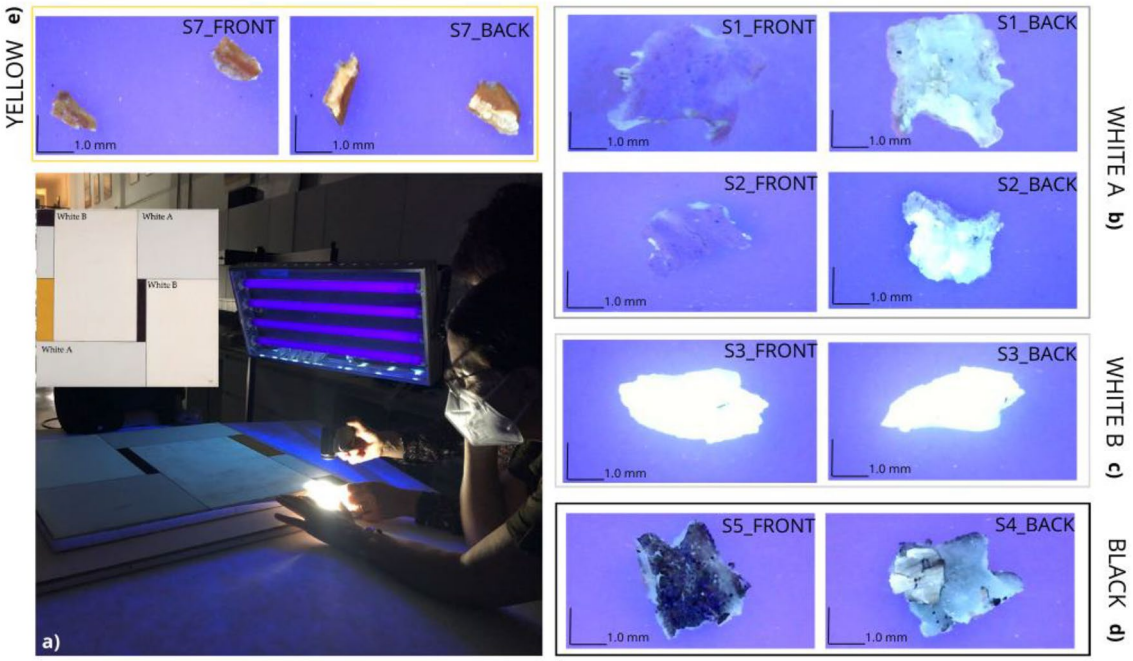

Fig. 3 Images acquired during the sampling campaign: **a** in situ observation with Wood's lamp and digital portable microscope in UV light; **b** images of samples 1 and 2 (white A) on front and back; **c** images of sample 3 (white B) on front and back; **d** images of sample 5 (balck area) on front and back; **e** images of sample 7 (yellow area) on front and back. The back of all samples and the front of sample 3 (white B) show a bright yellow UV fluorescence under UV light

recorded between 4000 and 400 cm^{-1} by performing 48 scans, with a resolution of 4 cm^{-1} [13].

The software used for data collection is Opus, while for spectra processing are Origin 9 and ThermoNicolet's OMNIC 6.0.

Raman spectroscopy coupled with microscopy (μ-Raman)

The analysis was carried out on all samples in order to identify the nature of the binding media and pigments and the presence of any additives in the paints or degradation products. The μ-Raman analysis was performed on all samples, except for samples 5 and 6, which could not be analysed as they are black in the visible region of the spectrum and absorb the excitation laser beam [11, 14–18].

Raman spectra were retrieved using a ThermoScientific™ DXR3™ dispersive Raman system (Waltham, MA, USA) equipped with an Olympus microscope. The experimental parameters were: laser wavelengths of 785 nm, laser power of 5 mW, and full range grating 50–3350 cm^{-1}. A 10× objective and a slit aperture of 25 μm were used to obtain more representative spectra from the samples. The total acquisition time for each spectrum was 120 s. ThermoScientific™ OMNIC™ 34.3 software (version 3, Waltham, MA, USA) was used to operate the DXR3™ Raman microscope and to collect the spectra. Raman spectra were compared with the instrument's internal library and literature for peak assignment.

Gas chromatography–mass spectrometry (GC–MS)

GC–MS analysis was performed on all samples in order to identify the nature of the binding media and the presence of organic additives in the paints or oxidation and degradation products.

GC–MS analyses were performed following a well-established procedure, tailored for modern and contemporary oil paints [19–25]. A Thermo Scientific™ TRACE™ 1300 Series GC System equipped ISQ 7000 MS with a quadrupole [26–30] analyzer by ThermoFisher Scientific was used. Samples were auto-injected in splitless mode at 280 °C and GC separation was performed on a fused silica capillary column DB–5MS Column (30 m length, 0.25 mm, 0.25 μm—5% phenyl methyl polysiloxane), using helium as the carrier gas (1 mL/min flow rate). The transfer line was at 280 °C and the MS source temperature was 300 °C. The temperature was programmed from 80 °C to 315 °C with a ramp of 10 °C, held isothermally for 2 min; the total runtime was 27.50 min. The MS run in Full Scan mode (m/z 40–650) with a speed of 0.2 scan/sec. The volume injected was 1 μL and the solvent delay was set at 8 min. Electron Ionisation energy was 70 eV. Data were processed with Chromeleon

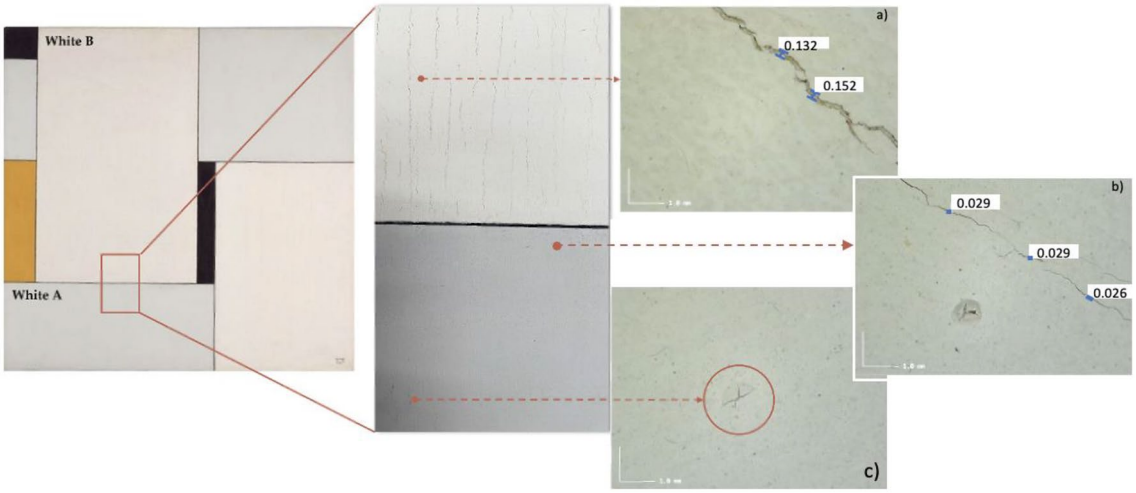

Fig. 4 Different crack patterns were observed: **a** ordered cracks in a semi-connected network; **b** short, random and unconnected cracks; **c** star- or cross-shaped cracks

chromatography studio. The compounds were identified as methyl ester (following a transesterification reaction) by comparison with the NIST. The samples were prepared with the derivatizing agent MethPrepII™, a methyl-esterifying agent consisting of a 5% solution of m(Trifluoromethyl) phenyltrimethylammonium hydroxide in methanol. Quantitative analysis was achieved using nonadecanoic acid as the internal standard and calculating ratios between the most important fatty acids (myristic, palmitic, stearic, azelaic, suberic, sebacic). Palmitic to stearic acid ratio (P/S) is commonly used to identify the type of oil; azelaic to palmitic ratio (A/P) to distinguish drying oils from egg lipids; A/Sub (ratio of azelaic to suberic acid) to provide an assessment of any preheating processes that may have occurred in the preparation of the oil; D% (total percentage of dicarboxylic acid, represented by azelaic, suberic and sebacic acids) to provide information on the degree of oxidation of oil; O/S (oleic to stearic acid ratio) may indicate the maturity of oils [5, 6, 30–39].

Results and discussion

This section illustrates the results obtained by the multi-analytical approach based on non-invasive analyses (digital portable microscopy and multiband imaging) and micro-invasive analyses (ATR-FTIR, μ-Raman, GC–MS) techniques. This hybrid experimental approach allowed to obtain useful information on the physical, chemical and mechanical aspects related to Vantongerloo's painting conservation.

The most significant data are reported in this section, while all the analyses are presented in the Additional file 1.

Study of cracks and morphology

A detailed study of cracks and their morphology using non-invasive techniques allowed the characterisation of different crack patterns in individual colour areas (white A, white B, yellow and black), as a function of orientation, length, width and appearance of the crack edges.

Three different crack patterns were observed in the white areas (white A, white B):

- short, random and unconnected cracks were observed in the dark white areas (white A). They had sharper edges and were less open ($\bar{x}$ 0.035 mm) than those observed in white B ($\bar{x}$ 0.114 mm);
- short, sharp-edged cracks resulting in a star- or cross-shaped pattern were identified in the protrusions emerging from the painting in white A (Fig. 4);
- ordered crack pattern parallel to the longest side of the painting, and consisting of semi-connected cracks, forming some square islands and with irregular-rounded edges was identified in the lighter white areas (white B).

Two different crack patterns were identified in the black and yellow areas. Whereas parallel sharp-edged cracks forming an ordered pattern perpendicular to the longest side of the painting (vertical direction) were identified in the yellow area, short cracks with irregular rounded edges randomly distributed and not visible to

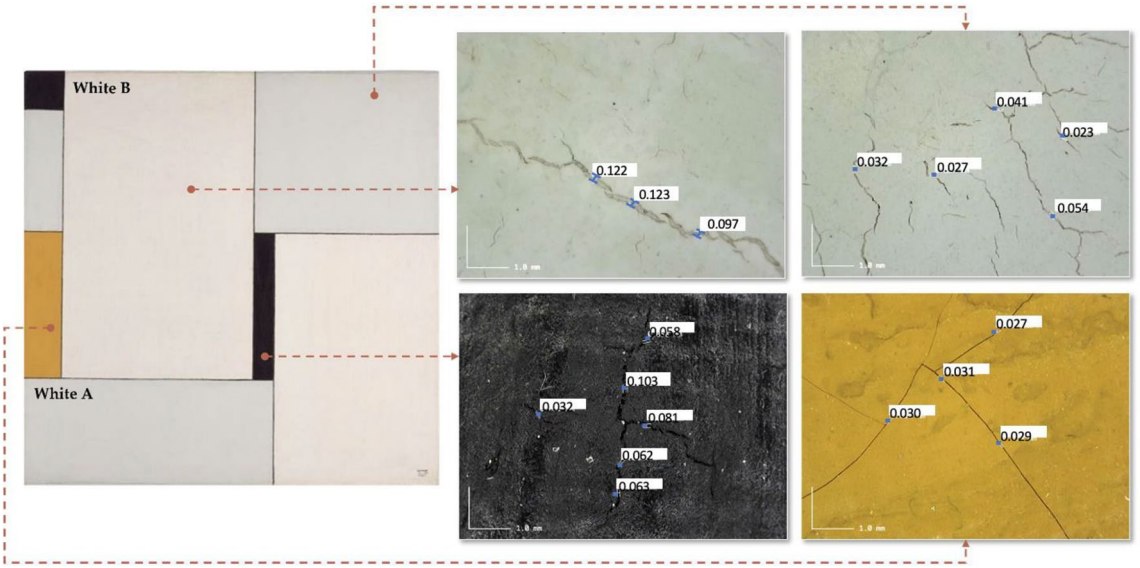

Fig. 5 Different crack patterns by colour area. Differences in the edges and widths can be observed

the naked eye were observed with the microscope in the black area instead.

According to such observations, white B and black areas present cracks with irregular-rounded edges, while white A and the yellow area present sharp cracks. In terms of crack width, the widest cracks are found in white B ($\bar{x}$ 0.114 mm), followed by the black colour ($\bar{x}$ 0.066 mm) and white A ($\bar{x}$ 0.035 mm), while those with the narrowest openings are found in the yellow area ($\bar{x}$ 0.029 mm) (Fig. 5).

Multiband imaging

Figure 6 shows schematically the images obtained through the different multiband techniques applied to Vantongerloo's painting. Additional files illustrate Figures S1-5

Considering the different conditions observed in the white areas, the identification of the white pigment(s) used was a priority to understand the different failure mechanisms behind the damage observed. Two white colours can be observed in the five different rectangles in Vantongerloo painting. While their appearance in VIS is rather similar, two distinct colours were observed in UVR: the darker white (white A) showed a middle grey, which may indicate a mixture of two whites, or a mixture of a white with another (or more) pigment(s); while the brightest white (white B) exhibited a relatively bright response in UVR (Fig. 7). Indeed, UVR imaging allows the distinction among white pigments: considering modern white pigments, titanium white and zinc white have a strong UV absorbance being identifiable for appearing very dark in the UVR image, especially when compared to other white pigments, namely lead white and lithopone, which appear brighter (Additional file 1: Figure S.3) [10, 40].

UVL images showed a similar response: three with a blueish-grey hue (white A) and two other very luminescent rectangles (white B) (Additional file 1: *Figure S.4*). Furthermore, the reflected IR image suggested the use of a white mixture with some other colours in the darker whites (white A). IRT confirmed this hypothesis as this type of imaging allows detailed observation of cracks and the internal condition of the paint layers (Additional file 1: Figure S5). In fact, the condition of both whites was different from the type of degradation observed: Fig. 8 highlights the presence of protrusions in the white A area, while Fig. 9 shows the cracks created in the white B area. The greyish one (white A) had a uniform and compact appearance, being highly absorbent and capable of blocking almost the whole radiation and no cracks can be observed on it. The brightest one (white B) evidenced a singular cracking, visible thanks to the radiation passing through it.

By comparing multiband images, it was possible to trace a preliminary hypothesis about the palette used by the artist [10]. As stated, UVR and UVL revealed a bright white which could be either lead white $(PbCO_3)_2 \cdot Pb(OH)_2$ either lithopone (30% ZnS + 70% $BaSO_4$) or a mixture of both in white B areas [10, 41, 42]. The darker hue in white A areas was difficult to determine, making the use of a mixture of elements highly possible.

Black pigments do not reveal any specific issue. Instead, the degradation of yellow was particularly

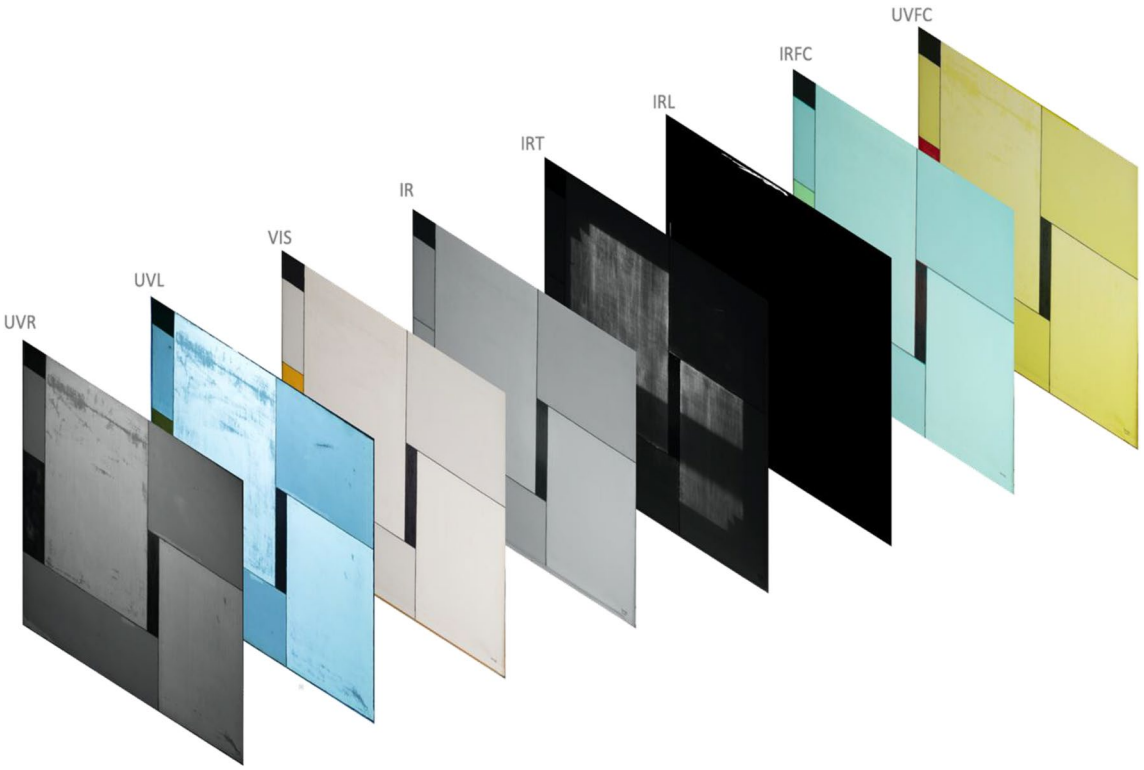

Fig. 6 Multiband images of the painting ordered by wavelength. Hybrid images such as UVFC and IRFC are reported as Additional file: Figures S1, S2

interesting. The three most common modern inorganic yellow pigments were considered: cadmium, chrome, and cobalt-based yellows. UVL suggested that cobalt could be the main pigment present in the yellow area given its greenish hue [4, 10, 40], although a mixture with other pigments or colourants should not be ruled out (Fig. 10). Cadmium yellow was not considered, because IRL shows no glowing over the yellow area [43–45].

This technique also revealed a particular luminescence in the upper and lower margins of the white A area that is typical of white titanium paint in rutile form. These areas are therefore made up of another type of white and could indicate repainting.

Chemical investigation of artist's materials

White A

ATR-FTIR, μ-Raman and GC–MS (Additional file 1: Figure S6–S13) analyses were performed on samples 1 and 2 in white A area (darker white).

In both samples, ATR-FTIR and μ-Raman results indicate the main presence of oxidised drying oil(s), metal soaps and calcite [14–18]. The detected metal soaps are most likely zinc soaps, according to their typical IR absorptions at 1727 (ν-C=O), 1535(δ-COO^-), 1462(δCH_2) and 1417(ν-COO^-) cm^{-1} (Fig. 11) [6, 36, 46–50]. Moreover, the presence of zinc white (ZnO) and/or a Zn-based compound could be assumed by the broad band at 600–400 cm^{-1}, assigned to white pigment.

As concerns the identification of white pigment(s), the μ-Raman analyses performed on the pictorial layer of the front of sample 2 showed the characteristic peaks of titanium dioxide (TiO_2) in anatase form (141, 394, 516,635 cm^{-1}) and peaks related to the presence of $BaSO_4$ (1103,1055,981, 632 cm^{-1}), probably used as additive. The spectrum of the front of sample 1 showed the characteristic peaks of titanium dioxide (TiO_2) in rutile form (141, 230, 447, 606 cm^{-1}). [51–53] (Fig. 12).

Titanium dioxide (TiO_2) in anatase form was also detected in the preparatory layers of both the back of samples 1 and 2 with a small peak at 438 cm^{-1} related to the presence of zinc oxide in the preparatory layer (Fig. 3).

The pigments detected by spectroscopic analysis confirmed the hypothesis formulated by the cross-sectional observation of multiband images, i.e. a mixture of titanium white with zinc white and other additives.

Thanks to GC chromatographic analysis, it was possible to identify and quantify the organic fraction of samples 1 and 2, underlining similarities and important

Fig. 7 UVR image of the case study confronted with the shades obtained from different control white pigments (titanium, lead, lithopone and zinc-based compounds). Considering the brighter response of white B (area delimited by red dots), lead or lithopone (or even a mixture of both) seems to be the white pigment used

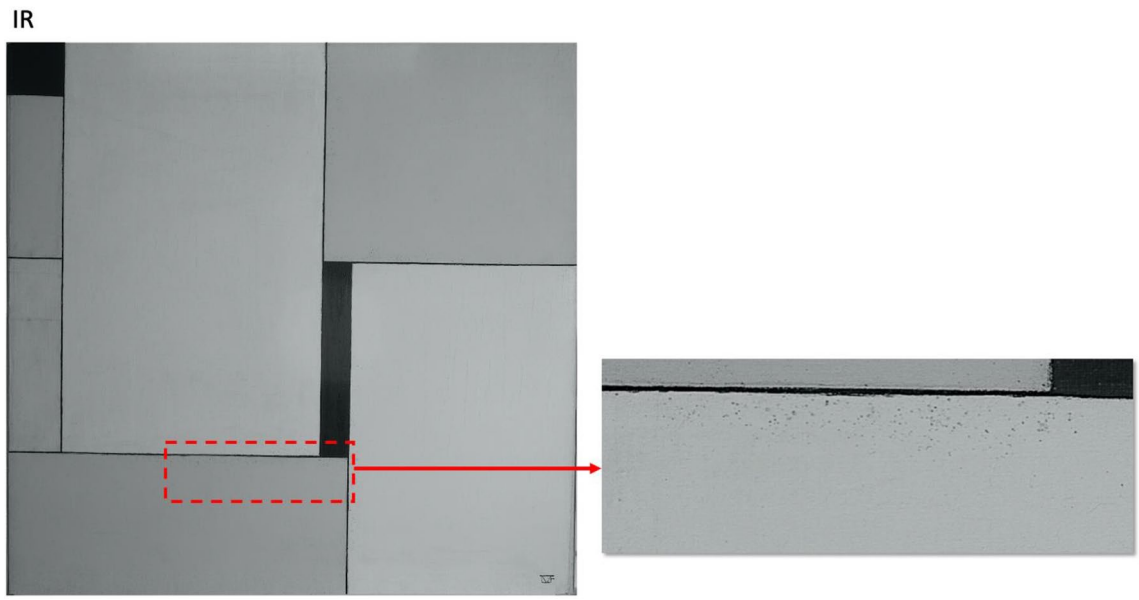

Fig. 8 IR image confirms the presence of protrusions in the white A area

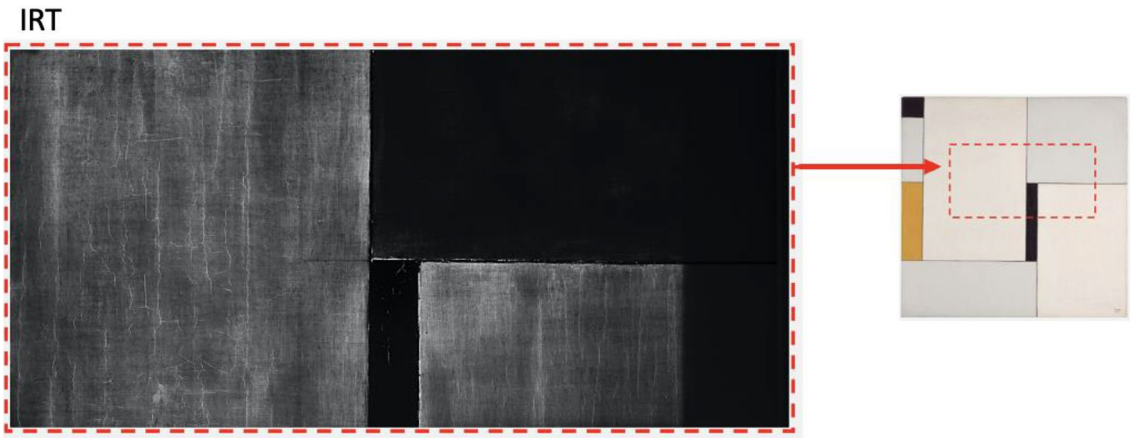

Fig. 9 IRT detail of the painting. While cracks can be observed as radiation passes through in white B areas, IR radiation is completely blocked in white A, showing a very absorbent and dark area, where no cracks are observed

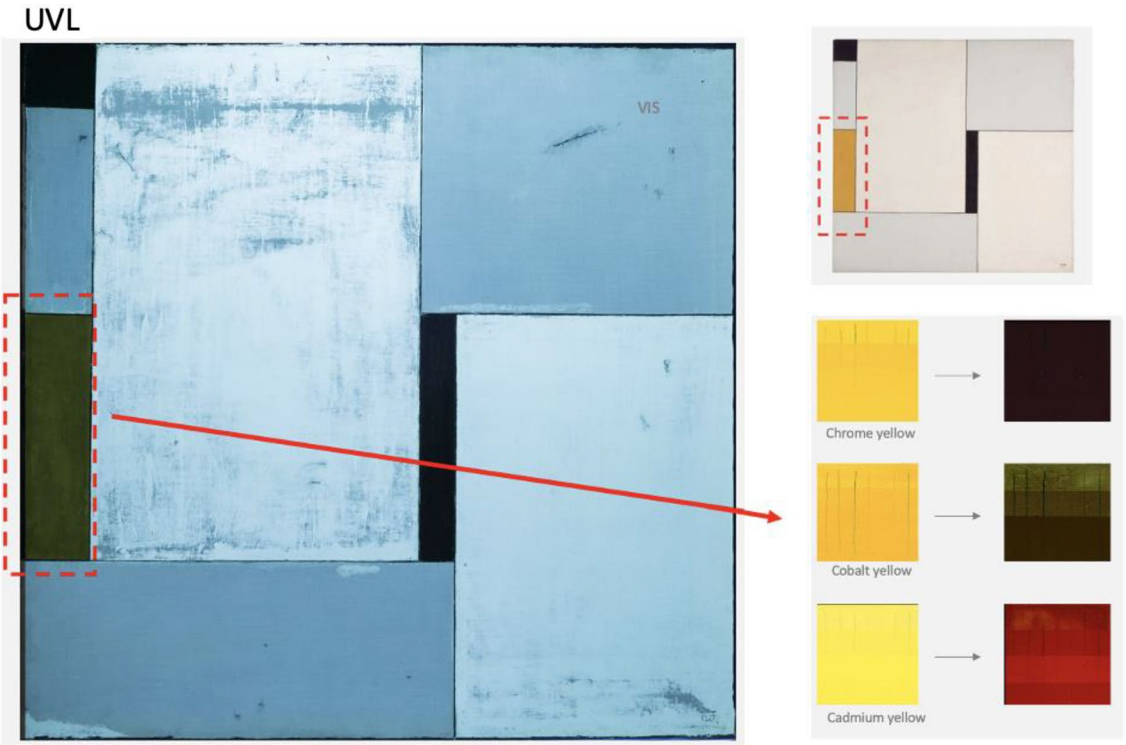

Fig. 10 UVL image of the painting compared with the shades obtained from different control yellow pigments (chrome, cobalt and cadmium-based pigments). Considering the dark green response of yellow (area delimited by red dots), cobalt yellow (or a mixture with it) seems to be the yellow pigment used

differences in the paint composition (Table 1) (Additional file 1: Figure S.9-S.13).

– The presence of saturated short and long-chain fatty acids such as lauric, myristic, palmitic, and stearic acid, which are typical of the lipidic compound, confirmed the previous hypothesis of the use of drying oil in both paint samples. Similarly, dicarboxylic acids (such as adipic, suberic, azelaic, and sebacic acids) were detected, as the main oxidative degradation products formed as the fragmentation of triglycerides occurred in the cross-linked network. In addition, chromatograms showed the presence of oxidation products such as octanoic acid (oxo-, hydroxy,

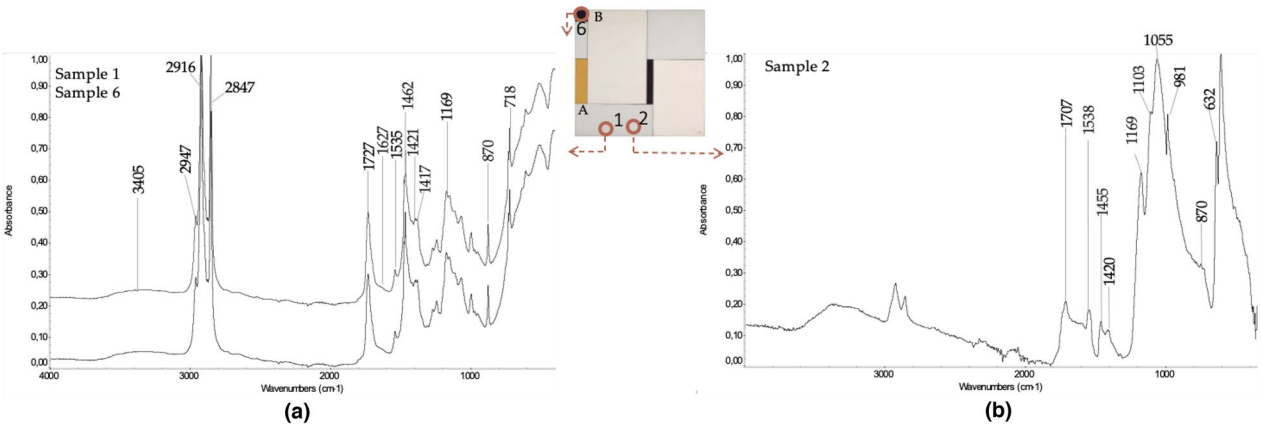

Fig. 11 ATR-FTIR spectra of: **a** samples 1 and 6 in which the characteristic peaks of drying oil calcite are reported; **b** sample 2 in which the characteristic bands of zinc soap and $BaSO_4$ are shown

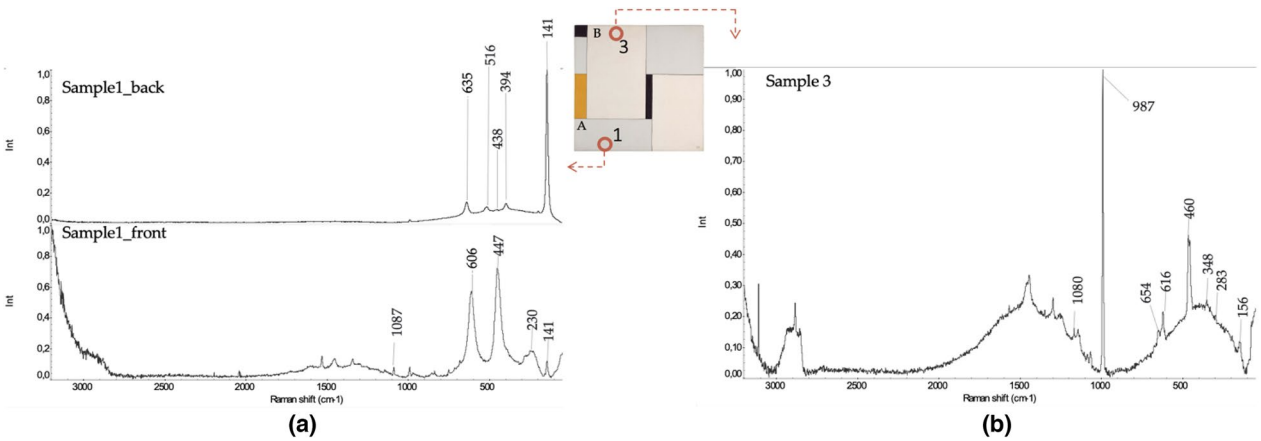

Fig. 12 μ-Raman analysis: **a** the spectra of sample 1 (white A) show the use of titanium white in the form of anatase on the back and rutile on the front of the sample; **b** the spectrum of sample 3 makes it possible to determine the use of lithopone as a pigment in white B area

epoxy-) and octadecanoic acids caused by oxidative cleavage of UFAs.

- Furthermore, castor wax, a waxy compound also called hydrogenated castor oil, was detected in both samples thanks to its typical markers [19] (Fig. 13). This compound is generally added as a stabilizing agent or as a rheology additive to prevent the separation of the lipidic fraction in commercial artists' oil-based paints (i.e. oils and alkyd resins) [54–56].
- The molar ration values have confirmed the presence of cold-pressed siccative oil, much likely linseed oil (P/S = 1.51) for sample 2 [6, 19, 24, 30]. However, D% value (calculated as the sum of suberic, sebacic and azelaic acids) was unexpectedly low (14.21%) compared with the average value of dicarboxylic acids in the other samples analyzed (22.67%), as can be seen in Table 1. GC–MS analyses revealed a correlation between the high concentration of oleic acid (9.75%), the low content of dicarboxylic acid and the type of degradation observed in the previous research where zinc oxide was detected [32, 57–59]. Indeed, it was proved that when this pigment is present, the Zn metal ions preferably interact with unsaturated fatty acids to form a packed crystalline structure that traps the oleic acid carbon chains and forms zinc soap. This hypothesis is supported by the evidence of protrusions on the painting surface in white A, caused by the migration of metal soaps[23, 32, 46, 48, 57–60].
- For sample 1, the P/S ratio is 0.86. This value is in agreement with previous studies [19, 28, 29, 36, 48] where metal stearates were found as additives in commercial oil-based paints and/or formed upon hydrolysis of the oil film.
- Different is the composition for sample 1. Due to the simultaneous occurrence of castor wax, terephthalic acid and cerotic acid, an oil-modified alkyd resin

Table 1 List of compounds identified by GC–MS and their concentration calculated in percentage

	Identified compound	Sample				
		WHITE B		WHITE A	BLACK	YELLOW
		1	2	3	5	7
Fatty acid and other compounds	Adipic acid ME	√	–	–	√	–
	Pimelic acid diME	–	√	–	√	–
	Glycerol derivate	√	√	√	√	√
	Octanoic acid ME	–	–	–	√	–
	Glycerol derivate	√	√	√	√	√
	Suberic acid diME	2.17%	2.01%	7.88%	4.07%	7.26%
	Glycerol derivate	√	√	√	√	√
	Terephthalic acid diME	√	√	–	–	√
	Lauric acid ME	√	√	–	√	√
	Azelaic acid diME	9.49%	6.28%	11.13%	10.88%	10.72%
	Sebacic acid diME	0.65%	5.92%	7.40%	6.99%	1.67%
	Myristic acid ME	√	√	√	√	√
	Glycerol derivate	√	√	√	√	√
	Palmitic acid ME	37.02%	42.13%	34.64%	35.5%	34.28%
	Margaric acid ME	√	√	–	√	√
	Linoleic acid ME	2.15%	2.01%	3.22%	2.33%	3.44%
	Oleic acid ME	0.26%	9.75%	1.3%	3.68%	4.3%
	Linolenic acid ME	5.02%	4.09%	5.78%	5.24%	0.00%
	Stearic acid ME	43.24%	27.81%	29.01%	31.31%	38.33%
	Nonadecanoic acid ME	√	√	√	√	√
	12-hydroxy stearic acid ME	√	√	√	√	√
	12-methoxy stearic acid ME	√	√	√	√	√
	Glycerol derivative	√	√	√	√	√
	Arachidic acid ME	–	–	√	√	√
	Octadecanoic acid, 9,10-dihydroxy ME	√	√	√	√	–
	Tetradehydroabietic acid, 7-methoxy ME	–	–	–	√	–
	Octadecanoic acid, 9,10-oxy ME	–	–	√	√	–
	Behenic acid ME	√	–	–	√	–
	Tetracosanoic acid ME	√	–	√	√	√
	Cerotic acid ME	√	–	–	–	√
	Montanic acid ME	√	–	√	√	–
	Octadecanoic acid, 9,10-oxo- ME	–	√	–	√	–
Molar ration among fatty acids	A/P	0.26	0.15	0.30	0.32	0.31
	P/S	0.86	1.51	1.19	1.13	0.89
	A/Sub	4.36	3.12	1.41	2.67	1.47
	D/P	0.33	0.33	0.76	0.64	0.57
	O/S	0.01	0.35	0.04	0.12	0.11
	%D	12.31%	14.21%	26.41%	21.94%	19.65%

The reported results were calculated by the chromatograms of samples 1, 2, 3, 5, and 7. √ = present; – = not detected; A/P = (azelaic/ palmitic); D/P = (dicarboxylic/ palmtic); O/S = (oleic/stearic); %D = (sum of the percentages of the following dicarboxylic acids: suberic, azelaic and sebacic). ME = methyl ester; diME = dimethyl ester

might be expected [34, 56, 61, 62, 64]. Two hypotheses can be then formulated:

1. the sample was taken from an inpainting/ retouched area (where an alkyd resin containing titanium white in the form of rutile was used);
2. the binder consists of the early use of an oil-modified alkyd house paint.

	O/S	0.01	0.35	0.04	0.12	0.11
	%D	12.31%	14.21%	26.41%	21.94%	19.65%

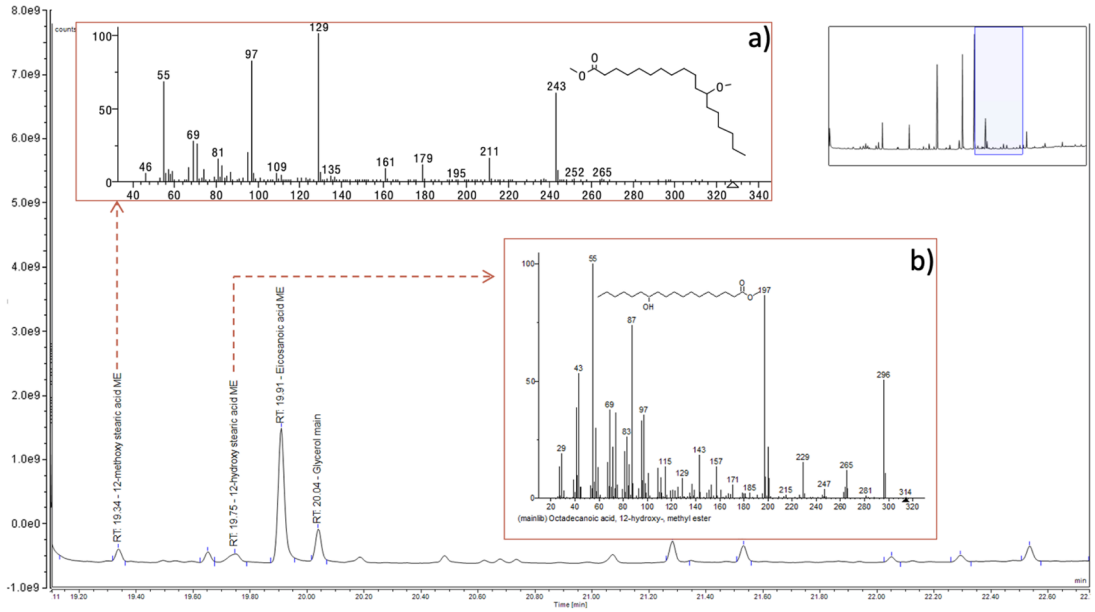

Fig. 13 GC–MS chromatogram of sample 1 in which castor wax was identified by its markers: **a** mass spectrum and chemical structure of 12-methoxy stearic acid ME; **b** mass spectrum and chemical structure of 12-hydroxy stearic acid ME

The first assumption could be confirmed by the fact that rutile has been commercialized since 1930 [51, 52, 65], so it is possible that it was not a material of the artist's choice considering that the painting dated back 1929. The hypothesis of house-painting was considered since the first oil-modified alkyd paints were made with linseed oil, castor wax and titanium dioxide as they guaranteed greater reproducibility, better colour, better-drying properties and film formation [66, 67].

White B

The white B area (lighter white) was analysed by ATR-FTIR and μ-Raman analysis was performed on the pictorial and preparatory layers of samples 3 and 4, which gave comparable results (Additional file 1: Figure S.14-S.21).

In the ATR spectra, the presence of drying oil (3445, 2951, 2915, 2847,1738, 1462, 1376, 1172 cm^{-1}), waxy material (1462, 729, 719 cm^{-1}), and calcite (1417, 1376, 884) was detected, as mentioned above [50, 68].

Concerning the white pigment, the very strong absorption at 988 cm^{-1} and weak at 654, 616, 460, 348 cm^{-1} in the μ-Raman spectra suggested the presence of lithopone [68] (Fig. 12 and Additional file 1: Fig. S19). This result was therefore in agreement with multiband imaging analysis (Figs. 7 and 10) where UVR and UVL images revealed the presence of lithopone.

Furthermore, the Raman spectra confirmed the presence of calcite due to its characteristic Raman peaks at 1080 and 288 cm^{-1} and the presence of drying oil. μ-Raman analysis performed on the back of samples, where the ground layer of the work of art was visible, confirmed the presence of the characteristic peaks of anatase, calcite and zinc white[14–18].

The chromatographic analysis performed on sample 3 (Table 1) confirmed the use of cold pressed linseed oil, according to the A/Sub (1.41) and P/S (1.19) molar ratios. In addition, castor wax markers [19] and oxidation fragments of octanoic and octadecanoic acid are detected. These oxidative scissions resulted in low concentrations of oleic acid (0.05 μg/mg) and high concentrations (26.41%) of dicarboxylic acids (adipic, suberic, azelaic, and sebacic).

In contrast to what was observed in white A, metal soaps and metal stearates were not detected by ATR. Thus, as observed by the study of morphology, no protrusions on the pictorial layer due to the migration of metal soaps have been detected [32, 57–59].

Black area

In the black area, two sampling points (samples 5 and 6) were selected to determine the material composition and to characterize the glossy layer observed on the surface.

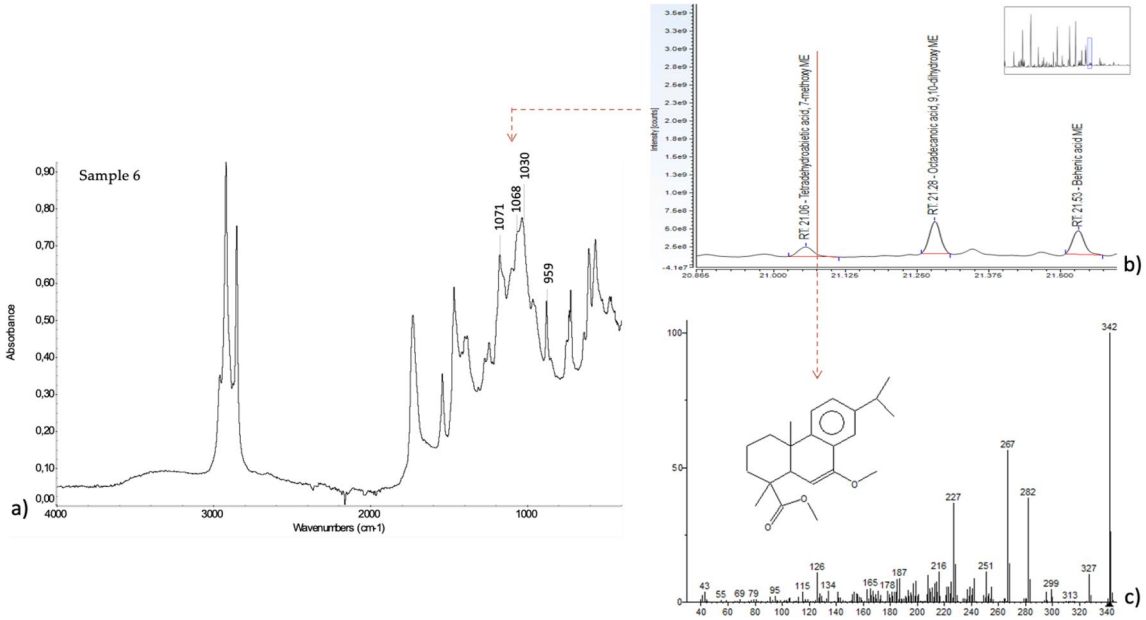

Fig. 14 Identification of natural resin in the black area: **a** ATR-FTIR analysis of sample 6 shows the characteristic peaks attributable to a natural resin; **b** chromatographic analysis made it possible to observe the characteristic peaks corresponding to a terpenic component characteristic of rosin (tetradehydroabietic acid, 7-methoxy ME which is a derivative of abietic acid); mass plectrum e chemical structure of tetradehydroabietic acid, 7-methoxy ME

FTIR-ATR spectra of black samples 5 and 6 showed the presence of oil (3401, 2951, 2915, 2847,1737, 1461, 1377, 1172 cm^{-1}), metal soap (1540, 1417 cm^{-1}), wax (1462, 729, 719 cm^{-1}), and calcite (1417, 867 cm^{-1}) (Fig. 10) [6, 29, 35, 48, 64]. Moreover, ATR spectrum of sample 6 also highlighted the presence of natural resin (1171, 1068–1030, 959 cm^{-1}) [56] (Fig. 14), corroborated by the detection of tetradehydroabietic acid, 7-methoxy ME in the GC–MS analysis. This compound is a derivative of abietic acid, occurring after oxidation [56] and can be found in terpenic materials, such as colophony or rosin [57, 58]. As reported in the literature, colophony has been widely used in commercial artists' paints as a thickener [17, 24, 69, 70]. Nevertheless, terpene-based material could belong to a varnish layers placed on the pictorial layer, which would explain the previously mentioned glossy paint layer [24, 49] (Additional file 1: Figure S.22-S.29).

Yellow area

The yellow area was analysed by performing ATR-FTIR, μ-Raman, and GC–MS on sample 7 (Additional file 1: Figure S.26-S.29).

ATR and μ-Raman analysis of sample 7 confirmed, as previously registered, the use of wax and oil as a binder, calcite as a filler, and the occurrence of metal soaps [6, 31, 48].

As far as the yellow colouration, it was assumed the presence of yellow pigment NY24, also known as Gamboge, mixed with Cobalt Yellow thanks to their characteristic Raman peaks (Fig. 15), respectively; at 1634 m, 1594 s, 1437 m, 1387w, 1329w, 1256 m, 1215w cm^{-1}, and 1398w, 1329 s, 1256w, 837 m, 821 s, 305 s, 276 m [17, 41, 42]. The presence of a cobalt-based pigment was also hypothesized by multiband imaging analyses that also assumed a mixture of yellow pigment, which was later confirmed by Raman analyses. Anatase (639, 516, 396, 143 cm^{-1}), zinc (440 cm^{-1}) and calcite (1087, 713, 283, 156 cm^{-1}) were further identified.

GC–MS analysis confirmed the presence of the main oxidative degradation products that formed as the fragmentation of triglycerides [5, 31, 33, 37, 38, 55, 60, 71, 72] and the presence of castor wax, as seen in Table 1 [19].

Correlation between morphology and chemical observations

Detailed condition reports over a 20-year time frame have revealed different crack patterns as a function of colour areas, being the white areas the most obvious example of selective damage: whereas white A (darker white) showed localized short, random and unconnected cracks and protrusions, white B areas (lighter white) showed ordered and semi-connected cracks.

In such a compact and neat painted surface, multi-band imaging analyses were essential to obtain

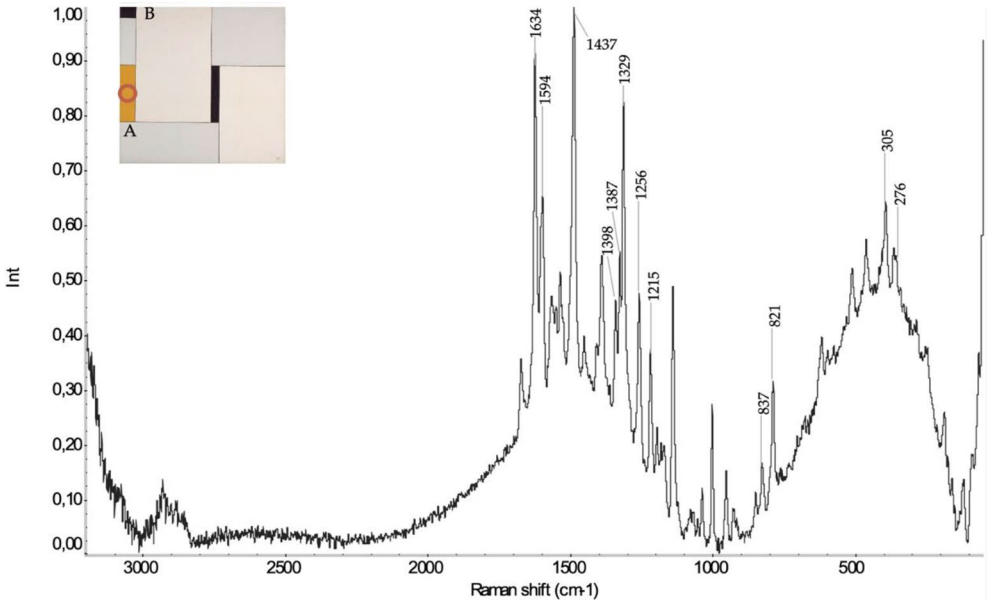

Fig. 15 µRaman spectrum of sample 7 on the yellow area: the main peaks related to the presence of the yellow pigment NY24, also known as Gamboge, mixed with Cobalt Yellow, are highlighted

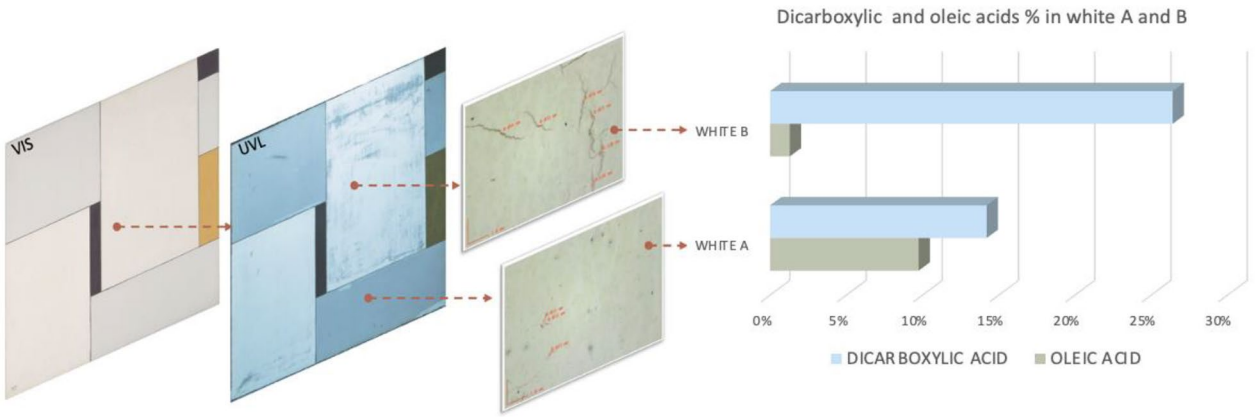

Fig. 16 Summary of the hybrid experimental approach carried out, which allowed to show the effects of pigment-medium interaction in the case study under consideration

preliminary indications on the pigments used. UVR imaging suggested the use of lead white or lithopone or a mixture of both as the main pigment in white B areas. This hypothesis was later confirmed by the µ-Raman technique, which made it possible to identify titanium dioxide (TiO_2) in the form of anatase in white A areas and lithopone in white B.

In addition, the analyses confirmed the presence of a preparatory layer composed of anatase (TiO_2), zinc oxide (ZnO) and calcite ($CaCO_3$) mixed in drying oil.

The characterisation of the organic compounds pointed out the use of commercial oil paints typical of the twentieth century. It was assumed the use of cold-pressed linseed oil with the addition of several additives, such as stabilizers (castor wax), dispersants (metal soaps), and thickeners (colophony).

Besides, the white paint in sample 1 has a different composition: terephthalic acid, castor wax and cerotic acid, among other compounds, suggested the use of an alkyd-based resin. It could either be a repaint (although the 2003 and 2015 conservation reports make no mention to it) or one of the earliest examples of oil-modified alkyd house paint. The latter was marketed in the summer of 1929 and improved to its most famous formulation, offered to the industrial trade in May 1931 by DuPont: Dulux GA-11. This was a 62% modified alkyd resin with linseed oil, additive with castor wax, pigmented with Titanox B (mix of titanium dioxide in the form of rutile

and anatase), and used for decorative purposes [66, 67, 73].

Having confirmed by spectroscopic analyses the different composition of the two white areas used by the artist (TiO_2 in white A and $BaSO_4$ + ZnS in white B), it is possible to state that the different damage patterns observed in this painting have been governed by the intrinsic nature of the painting materials and are not necessarily environmentally-induced.

- The protrusions identified in white A areas by the first non-invasive analyses were subsequently investigated. They are caused by the presence of zinc metal soaps, detected by the ATR-FTIR spectra (Fig. 1), and characterized by significantly higher concentrations of oleic acid (Table 1). This degradation phenomenon is caused by the interaction between the pigment and the oil binder: Zinc oxide present in the preparatory layer forms a packed crystalline structure that traps the oleic acid carbon chains and hinders their cross-linking. Over time, and favoured by certain environmental conditions, metal soaps migrate from the preparatory layer to the surface, leading to protrusions and unconnected cracks, as observed in this painting [32, 36, 46–48, 57].
- On the other hand, zinc sulphide and barium sulphate present in lithopone. used in white B areas led to a partial delamination of the surface. The chromatographic analysis shows a considerable formation of dicarboxylic acids and the formation of volatile compounds that make the pictorial layer brittle, favouring the penetration of water into the matrix, and leading to the dusty texture with ordered and semi-combined cracks [23, 36, 46, 63, 74, 75] (Fig. 16).

Conclusions

The starting point of this research was the singular morphology of cracks and protrusions observed in the different white areas of the case study under consideration, the Neoplasticist painting *Composition dans le cône avec couleur orange* by G. Vantongerloo (1929).

The aim of this study was to understand the causes that led to such degradation phenomena by correlating a thorough physical–chemical characterization of the palette used by Vantongerloo with a multiband analysis. This multi-analytical study made it possible to understand the physical, chemical and mechanical mechanisms involved in the damage patterns.

The multiband images provided precious preliminary information on the white pigment(s) used, which was later confirmed and supported by spectroscopic analyses. GC–MS analyses also strengthened the hypothesis that the degradation phenomena are closely linked to the chemical composition of the painting materials and in particular to the interaction between pigments and binding media.

In this sense, it was proved that random cracking and protrusions in white A areas were due to zinc soaps migrated from the preparatory layer, while the orderly and semi-combined cracking network was related to the interaction between lithopone and the lipidic binder and the significant formation of dicarboxylic acids and volatile compounds in white B areas.

This research opens up interesting new scenarios to be studied such as to what extent the type of siccation oil affects the interactions with metal ions in pigments and how the environment contributes to catalyse (or not) such processes.

Thus, the future goal will be a deeper understanding of the phenomena underlying the observed forms of degradation in order to design more informed conservation strategies.

Supplementary Information

The online version contains supplementary material available at https://doi.org/10.1186/s40494-024-01154-z.

Additional file 1. Additional Figures, Figures S1-S29.

Acknowledgements
The authors acknowledge the Institut Valencià d'Art Modern (IVAM) for allowing access to the collection.

Author contributions
F.C.I: conceptualization, data curation, investigation, writing (original draft), methodology revision; M.G: investigation, methodology, data curation, writing (original draft), revision; M.A.H: investigation, methodology, revision; A.M.G-C: investigation, methodology; M.T.M: resources, supervision; L.F-L: conceptualization, investigation, resources, funding, supervision, methodology, revision.

Funding
This research was carried out in the framework of PID 2019-106616 GB-100 project granted by MCIN/ AEI /https://doi.org/10.13039/501100011033 Theauthors acknowledge "Patto per Venezia"—Municipality of Venice for funding-part of the instrumentation used for the characterisation of heritage samples.

Availability of data and materials
Not applicable.

Declarations

Ethics approval and consent to participate
Not applicable.

Competing interests
The authors declare no conflict of interest.

Received: 15 November 2023 Accepted: 19 January 2024
Published online: 18 March 2024

References

1. Veen L. Piet Mondrian on the principles of neo–plasticism. Int J Art Art History. 2017;5(2):1–12. https://doi.org/10.15640/ijaah.v5n2a1.
2. Wallace IH. Piet Mondrian: the evolution of his neo-plastic aesthetic 1908–1920. Univ Br Columbia J. 1968. https://doi.org/10.14288/1.0104386.
3. Knight TW. Transformations of De Stijl Art: the Paintings of Georges Vantongerloo and Fritz Glarner. Environ Plann B Plann Des. 1989;16(1):51–98.
4. Fuster-López L, Herrero-Cortell MA, Izzo FC, García-Castillo AM, Picollo M, Cucci C, Martinez-López M. Selective cracks: Mapping damage from pigment-medium interaction in three neo-plastic oil paintings. Working Towards a Sustainable Past. ICOM-CC 20th Triennial Conference Preprints, Valencia, 2023.
5. Tumosa CS, Mecklenburg MF. The influence of lead ions on the drying of oils. Stud Conserv. 2005;50(sup1):39–47. https://doi.org/10.1179/sic.2005.50.supplement-1.39.
6. Mecklenburg MF, Kékicheff P, Roland T, Egele A, Favier D, Tranchant L, Schoeder S, Izzo FC, Fuster-López L, Andersen CK, Scharff M. Relationships between chemical and physical alterations of historical oil-based pictorial paintings: craquelures and metal ion-migration. From Soft Matter to Biophysics 2023. 2023;Book of ab: p.29.
7. Warda J. The AIC guide to digital photography and conservation documentation. Washington, DC: Foundation of the American Institute for Conservation of Historic and Artistic Works. 2011.
8. Cosentino A. Practical notes on ultraviolet technical photography for art examination. 2015; 21.
9. Cosentino A. Identification of pigments by multispectral imaging; a flowchart method. Herit Sci. 2014;2(1):1–12.
10. Herrero-Cortell MA, Raich M, Artoni P, Madrid Garcìa JA. Caracterización de pigmentos históricos a través de técnicas de imagen, en diversas bandas del espectro electromagnético. Ge-Conservación. 2022;22:58–75.
11. Volpin S, Appolonia L. Le analisi di laboratorio applicate ai beni culturali artistici policromatici, Collana i Talenti. Padova, 2002.
12. Matteini M, Moles A. Scienza e restauro. Metodi d'indagine, 7th ed., vol. Arte e restauro. 1994.
13. Skoog DA, Holler FJ, Crouch SR. Chimica analitica strumentale, II edition. Napoli, 2009.
14. Tuschel D. Raman spectroscopy of oil shale. Spectroscopy (Santa Monica). 2013;28(3).
15. Dennis A. Raman spectroscopy of edible oils and fats. pp. 1–2, 2007, [Online]. Available: http://www.perkinelmer.com/PDFs/downloads/APP_RamanSpectroscopyOfEdibleOilsAndFats.pdf.
16. Vaskova H, Buckova M. Multivariate study of raman spectral data of edible oils. WSEAS Trans Environ Dev. 2018;14:226–32.
17. Burgio L, Clark RJH. Library of FT-Raman spectra of pigments, minerals, pigment media and varnishes, and supplement to existing library of Raman spectra of pigments with visible excitation. Spectrochim Acta Part A Mol Biomol Spectrosc. 2001. https://doi.org/10.1016/S1386-1425(00)00495-9.
18. Vagnini M, Gabriel F, Daveri A, Sali D. Handheld new technology Raman and portable FT-IR spectrometers as complementary tools for the in situ identification of organic materials in modern art. Spectrochim Acta A Mol Biomol Spectrosc. 2017;176:174.
19. Izzo FC. 20th century artists' oil paint:a chemical-physical survey. PhD thesis, no. University OF Ca' Foscari, Venice, 2011.
20. Fuster-López L, Izzo FC, Piovesan M, Yusá-Marco DJ, Sperni L, Zendri E. Study of the chemical composition and the mechanical behaviour of 20th century commercial artists' oil paints containing manganese-based pigments. Microchem J. 2016;124:962–73. https://doi.org/10.1016/j.microc.2015.08.023.
21. Fuster-López L, Izzo FC, Damato V, Yusà-Marco DJ, Zendri E. An insight into the mechanical properties of selected commercial oil and alkyd paint films containing cobalt blue. J Cult Herit. 2019;35:225–34. https://doi.org/10.1016/j.culher.2018.12.007.
22. Caravá S, RoldánGarcía C, Vázquez de Agredos-Pascual ML, Murcia Mascarós S, Izzo FC. Investigation of modern oil paints through a physico-chemical integrated approach. Emblematic cases from Valencia, Spain. Spectrochim Acta A Mol Biomol Spectrosc. 2020;240:30–2. https://doi.org/10.1016/j.saa.2020.118633.
23. Vila A et al. Picasso 1917: an insight into the effects of ground and canvas in the failure mechanisms in four artworks. Conservation of Modern Oil Paintings, pp. 245–253, 2019, https://doi.org/10.1007/978-3-030-19254-9_18.
24. Izzo FC, Källbom A, Nevin A. Multi-analytical assessment of bodied drying oil varnishes and their use as binders in armour paints. Heritage. 2021;4(4):3402–20. https://doi.org/10.3390/heritage4040189.
25. Gomez Lobon M, et al. A study of cadmium yellow paints from Joan Miró's paintings and studio materials preserved at the Fundació Miró Mallorca. Herit Sci. 2023;11(1):1–16. https://doi.org/10.1186/s40494-023-00987-4.
26. Van der Berg JDJ. Analytical chemical studies on traditional linseed oil paints, thesis, University of Amsterdam, 2002.
27. Cooper A, Burnstock A, Van der Berg KJ, Ormsby B. Water sensitive Oil Paints in the 20TH century, A study of the distribution of water-soluble degradation products in Winsor & Newton Artist' Oil Color paint swatches, with case studis from Tate's collection. Issue in Contemporary Oil Paint, Book of Abstract, Cultural Heritage Agency, Ministry of Education, Culture and Science, 2013.
28. Izzo FC, Ferriani B, Van den Berg KJ, Van Keulen H, Zendri E. 20th century artists' oil paints: the case of the Olii by Lucio Fontana. J Cult Herit. 2014;15(5):557–63. https://doi.org/10.1016/j.culher.2013.11.003.
29. Izzo, F.C., van den Berg, K.J., van Keulen, H., Ferriani, B., Zendri, E. (2014). Modern Oil Paints – Formulations, Organic Additives and Degradation: Some Case Studies. In: van den Berg, K., et al. Issues in Contemporary Oil Paint. Springer, Cham. https://doi.org/10.1007/978-3-319-10100-2.
30. Studies C, Izzo FC, Van Den Berg KJ, Van Keulen H, Ferriani B, Zendri E. Issues in Contemporary Oil Paint, 2014. https://doi.org/10.1007/978-3-319-10100-2.
31. Tumosa CS, Mecklenburg MF. Oil Paints: The Chemistry of Drying Oils and the Potential for Solvent Disruption," New Insights into the Cleaning of Paintings: Proceedings from the Cleaning 2010 International Conference, Universidad Politecnica de Valencia and Museum Conservation Institute, no. November 2010, pp. 51–58, 2013, [Online]. Available: https://repository.si.edu/bitstream/handle/10088/20489/11.Tumosa.SCMC3.Mecklenburg.Web.pdf?sequence=1&isAllowed=y.
32. Osmond G. Zinc white: a review of zinc oxide pigment properties and implications for stability in oil-based paintings. AICCM Bull. 2012;33(1):20–9. https://doi.org/10.1179/bac.2012.33.1.004.
33. Tumosa CS, Meckelnburg MF. Weight changes on oxidation of drying and semi-drying oils. Collection Forum. 2003;18(1–2):116–23.
34. Omari A, Mgani QA, Mubofu EB. Fatty acid profile and physico-chemical parameters of castor oils in Tanzania. Green Sustain Chem. 2015;5(4):154.
35. Burnstock A, Ormsby B, Schar M, Carlyle L. Conservation of Modern Oil Paintings. 2019. https://doi.org/10.1007/978-3-030-19254-9.
36. Sawicka L, Izzo FC, Van der Berg KJ, Burnstock A. Metal soap Efflorescence in Contemporary Oil Painting, Iusses in Contemporary Oil paint, book of Abstract. Cultural Heritage Agency, Ministry of Education, Culture and Science, 2013.
37. Lazzari M, Chiantore O. Drying and oxidative degradation of linseed oil. Polym Degrad Stab. 1999;65(2):303–13. https://doi.org/10.1016/S0141-3910(99)00020-8.
38. Mallegol J, Lemaire J, Gardette J. Drier influence on the curing of linseed oil. Progress Organic Coating. 2000;39:107–13.
39. Juita B, Dlugogorski EZ, Kennedy E, Mackie J. Oxidation reactions and spontaneous ignition of linseed oil. Proc Combustion INstitute. 2011;33:2625–31.
40. Herrero-Cortell MA, Creus MR, Artoni P. Multi-band technical imaging in the research of the execution of paintings. The case study of the portrait of Carlos IV, by Francisco de Goya. Geconservación. 2018;14:5–15.
41. Caggiani MC, Cosentino A, Mangone A. Pigments Checker version 3.0, a handy set for conservation scientists: a free online Raman spectra database. Microchem J. 2016;129:123–32. https://doi.org/10.1016/j.microc.2016.06.020.
42. Burrafato G, Calabrese M, Cosentino A, Gueli AM, Troja SO, Zuccarello A. ColoRaman project: Raman and fluorescence spectroscopy of oil, tempera and fresco paint pigments. J Raman Spectrosc. 2004;35(10):879–86. https://doi.org/10.1002/jrs.1229.
43. Thoury M, Delaney JK, de la Rie R. Near-infrared luminescence of cadmium pigments: in situ identification and mapping in paintings. Appl Spectrosc. 2011;65(8):939–51.

44. Sands S. On the Yellowing of Oils. Just Paint, pp. 1–11, 2019, [Online]. Available: https://www.justpaint.org/on-the-yellowing-of-oils/.
45. Note P. Yellowing of oils—update and new testing at the 5 year mark. no. Graph 1, pp. 1–7, 2021.
46. Steele LL. Effect of certain metallic soaps on the drying of raw linseed oil. Ind Eng. 1924;16:957.
47. Casadio F et al. Metal soaps in art: conservation and research. Springer International Publishing—Cultural Heritage Science, 2018, https://doi.org/10.1007/978-3-319-90617-1.
48. Izzo FC, Kratter M, Nevin A, Zendri E. A critical review on the analysis of metal soaps in oil paintings. ChemistryOpen. 2021;10(9):904–21. https://doi.org/10.1002/open.202100166.
49. Higgs S, Burnstock A. An investigation into metal ions in varnish coatings. pp. 123–140, 2019, https://doi.org/10.1007/978-3-319-90617-1_7.
50. Baij L, Hermans JJ, Keune K, Iedema P. Time-dependent ATR-FTIR spectroscopic studies on fatty acid diffusion and the formation of metal soaps in oil paint model systems. Angew Chem Int Ed. 2018;57(25):7351–4. https://doi.org/10.1002/anie.201712751.
51. Dal Santo V, Naldoni A. Titanium dioxide photocatalysis. 2018. doi: https://doi.org/10.3390/catal8120591.
52. van Driel B, et al. New insights into the complex photoluminescence behaviour of titanium white pigments. Dyes Pigm. 2018;155:14–22. https://doi.org/10.1016/j.dyepig.2018.03.012.
53. Curran M. The kinetics of fading: opaque paint films pigmented with alizarin lake and titanium dioxide. J Am Inst Conserv. 2018;23(2):114–29.
54. Ploeger R, Scalarone D, Chiantore O. The characterization of commercial artists' alkyd paints. J Cult Herit. 2008;9(4):412–9. https://doi.org/10.1016/j.culher.2008.01.007.
55. Mecklenburg MF, Tumosa CS, Vicenzi EP. The Influence of Pigments and Ion Migration on the Durability of Drying Oil and Alkyd Paints. New Insights into the Cleaning of Paintings: Proceedings from the Cleaning 2010 International Conference, Universidad Politecnica de Valencia and Museum Conservation Institute, no. November 2010, pp. 59–67, 2013. Available: https://repository.si.edu/bitstream/handle/10088/20490/12.Mecklenburg.SCMC3.Mecklenburg.Web.pdf?sequence=1&isAllowed=y.
56. Choe YA, Il Kim S, Ju KS. Synthesis and characterizations of high oil length alkyd resin with dehydrated castor oil and acrylic pimaric acid. Chem Phys Lett. 2022;805:139934. https://doi.org/10.1016/j.cplett.2022.139934.
57. Osmond G. Zinc soaps: an overview of zinc oxide reactivity and consequences of soap formation in oil-based paintings. 2019. https://doi.org/10.1007/978-3-319-90617-1_2.
58. Beerse M, Keune K, Iedema P, Woutersen S, Hermans J. Evolution of zinc carboxylate species in oil paint ionomers. ACS Appl Polym Mater. 2020;2(12):5674–85. https://doi.org/10.1021/acsapm.0c00979.
59. Giorgi L, et al. In-situ technical study of modern paintings - Part 2: Imaging and spectroscopic analysis of zinc white in paintings from 1889 to 1940 by Alessandro Milesi (1856–1945). Spectrochim Acta A Mol Biomol Spectrosc. 2019;219:504–8. https://doi.org/10.1016/j.saa.2019.04.084.
60. Simunkova MD, Khattab T, Wu J. Review of autoxidation ad driers. Progress Organic Coatings. 2012; 73.
61. Mallu SP, Roopa S, Somashekarappa H, Somashekar R. Studies on physico-mechanical and optical properties, and WAXS of castor oil based polyurethane/polyacrylates interpenetrating polymer networks. J Appl Polym Sci. 2005;95(3):764–73. https://doi.org/10.1002/app.21276.
62. Huyan Z, Ding S, Yu X, Liu X. Preparation and characterization of hydrogenated castor oil-based coating wax. Eur J Lipid Sci Technol. 2018;120(4):1–7. https://doi.org/10.1002/ejlt.201700444.
63. Patel VR, Dumancas GG, Viswanath LCK, Maples R, Subong BJJ. Castor Oil: properties, uses, and optimization of processing parameters in commercial production". Lipid insights. 2016;9:1–12. https://doi.org/10.4137/LPI.S40233.
64. Plenderleith HJ. The History of artists' pigments. Science Progress (1933), Vol. 38, No. 150 (1950), pp. 246–256 (11 pages), https://www.jstor.org/stable/43422835.
65. Learner A, Thomas JS, Smithen P, Krueger JW, Schilling RM. Modern paints uncovered: proceedings from the modern paints uncovered symposium. Los Angeles: Getty Conservation Institute, 2008, Los Angeles, http://hdl.handle.net/10020/gci_pubs/paints_uncovered.
66. Eric D, Price Clifford A. House Paints 1900–1960. History and Use, no. 2. 2010. Available: http://hdl.handle.net/1811/4918.
67. Derrick MR, Stulik DC, Landry JM. Infrared spectroscopy in conservation science. Los Angeles: Getty Conservation Institute, 2008, Los Angeles, 1999.
68. Rie R. Fluorescence of paint and varnish layer. Stud Conserv. 1982;27:65–108.
69. Källbom A, Nevin A, Izzo FC. Multianalytical assessment of armour paints-the ageing characteristics of historic drying oil varnish paints for protection of steel and iron surfaces in Sweden. Heritage. 2021;4(3):1141–64. https://doi.org/10.3390/heritage4030063.
70. Fjallstrom P, Andersson B, Nilsson C, Andersson K. Drying of linseed oil paints: a laboratory study of aldehyde emission. Ind Crops Prod. 2002;16:174–84.
71. Pizzimenti S, Bernazzani L, Tinè MR, Treil V, Duce C, Bonaduce I. Oxidation and cross-linking in the curing of air-drying artists' oil paints. ACS Appl Polym Mater. 2021;3(4):1912–22. https://doi.org/10.1021/acsapm.0c01441.
72. Croll S. Overview of development in the paint industry since 1930, Modern paints Uncovered. London, 2006.
73. Eumelen GJAM, et al. Computational modelling of metal soap formation in historical oil paintings: the influence of fatty acid concentration and nucleus geometry on the induced chemo-mechanical damage. SN Appl Sci. 2020. https://doi.org/10.1007/s42452-020-3038-z.
74. Banti D, Nasa JL, Tenorio A, Modugno F, Van Den KJ, Berg J. A moleculer study of modern oil paintings: investigating the role of dicarboxylic acids in the water sensitivity of modern oil paints", RSC Advances, vol. 11, 2018, https://doi.org/10.1039/C7RA13364B.
75. Hermans JJ, Keune K, Van Loon A, Iedema PD. Toward a complete molecular model for the formation of metal soaps in oil paints. pp. 47–67, 2019, https://doi.org/10.1007/978-3-319-90617-1_3.

Publisher's Note